

## Pseudogap, Superconducting Gap, and Fermi Arc in High- $T_c$ Cuprates Revealed by Angle-Resolved Photoemission Spectroscopy

Tepei Yoshida<sup>1\*</sup>, Makoto Hashimoto<sup>2</sup>, Inna M. Vishik<sup>2</sup>, Zhi-Xun Shen<sup>2</sup>, Atsushi Fujimori<sup>1</sup>

<sup>1</sup>*Department of Physics, University of Tokyo, Bunkyo-ku, Tokyo 113-0033, Japan*

<sup>2</sup>*Stanford Institute for Materials and Energy Sciences, SLAC National Accelerator Laboratory, 2575 Sand Hill Road, Menlo Park, CA 94025, USA*

We present an overview of angle-resolved photoemission spectroscopy (ARPES) studies of high-temperature cuprate superconductors aiming at elucidating the relationship between the superconductivity, the pseudogap, and the Fermi arc. ARPES studies of underdoped samples show a momentum dependence of the energy gap below  $T_c$  which deviates from a simple  $d$ -wave form, suggesting the coexistence of multiple energy scales in the superconducting state. Hence, two distinct energy scales have been introduced, namely, the gap near the node (characterized by  $\Delta_0$ ) and in the anti-nodal region (characterized by  $\Delta^*$ ). Dichotomy between them has been demonstrated from the material, doping, and temperature dependence of the energy gap. While  $\Delta^*$  at the same doping level is approximately material independent,  $\Delta_0$  shows a strong material dependence tracking the magnitude of  $T_{c,max}$ . The anti-nodal gap does not close at  $T_c$  in contrast to the gap near the node which follows something closer to a BCS-like temperature dependence. An effective superconducting gap  $\Delta_{sc}$  defined at the end point of the Fermi arc is found to be proportional to  $T_c$ 's in various materials.

KEYWORDS: high- $T_c$  superconductor, angle-resolved photoemission spectroscopy

### 1. Introduction

From the earliest studies of high- $T_c$  cuprate superconductors, the origin of the pseudogap has remained unresolved and has been considered as the most fundamental problem for understanding the mechanism of high- $T_c$  superconductivity. The central issue is whether the pseudogap is related to the superconductivity or is a distinct phenomenon from the superconductivity. In the former scenario, a possible origin of the pseudogap is preformed Cooper pairs lacking phase coherence.<sup>1,2)</sup> In that picture the pseudogap is a remnant of the superconducting gap into the phase-incoherent regime and reflects the intrinsic pairing tendency of the underlying electronic states. In the latter scenario, the pseudogap arises from a competing order<sup>3-5)</sup> or antiferromagnetic correlation.<sup>6,7)</sup>

It has been well known for more than 15 years that the pseudogap in the antinodal  $\sim(\pi,0)$

---

\*E-mail address: yoshida@wyvern.phys.s.u-tokyo.ac.jp

region increases with underdoping and finally becomes much larger than the BCS value of  $2\Delta \sim 4k_B T_c$  as observed by angle-resolved photoemission spectroscopy (ARPES)<sup>8)</sup> and tunneling spectroscopy.<sup>9)</sup> Such a large anti-nodal gap in the underdoped materials had sometimes been attributed to strong Cooper pairing. However, the energy gap measured by Andreev reflection,<sup>10)</sup> temperature-dependence of penetration depth,<sup>11)</sup> and Raman scattering of  $B_{2g}$  geometry,<sup>12,13)</sup> the latter of which probes the gap near the  $d$ -wave node and the former of which should be directly associated with superconductivity, exhibit different trends. That is, with underdoping, the gap magnitude near the node saturates around the optimal doping and then decreases or remains nearly constant, suggesting a different origin of the gap near the node from the anti-node. Stimulated by those experimental results, detailed investigations of the energy gap in the momentum space by ARPES have recently been performed extensively. An ARPES study of  $\text{Bi}_2\text{Sr}_2\text{CaCu}_2\text{O}_8$  (Bi2212) has revealed the presence of two distinct energy scales for the nodal and anti-nodal regions in the heavily underdoped regime.<sup>14)</sup> A similar “two-gap” behavior has been observed in the single-layer cuprates for under- and optimally-doped regions such as  $\text{La}_{2-x}\text{Sr}_x\text{CuO}_4$  (LSCO) and  $\text{Bi}_2\text{Sr}_2\text{CuO}_{6+\delta}$  (Bi2201).<sup>15–18)</sup> Also, a temperature-dependent angle-integrated photoemission study of LSCO has indicated two distinct energy and temperature scales of the gap.<sup>19)</sup> These observations are schematically illustrated in Fig. 1 as a two-gap picture, where a gap from competing order coexists with a superconducting gap. In this picture, the gap in the anti-node  $\Delta^*$  is sufficiently larger than the gap near the node  $\Delta_0$ , and the gap function shows a deviation from a simple  $d$ -wave form, indicating a crossover between the two kinds of gaps. When  $\Delta^*$  is comparable to or smaller than  $\Delta_0$ , the clear deviation may not exist. The existence of competing order, which has spatial modulations of the charge like checkerboard, has also been suggested by scanning tunneling spectroscopy studies (STM) on  $\text{Ca}_{2-x}\text{Na}_x\text{CuO}_2\text{Cl}_2$ .<sup>4)</sup> Furthermore, NMR studies have revealed two distinct temperature scales in the relaxation rate corresponding to the pseudogap temperature  $T^*$  and  $T_c$ .<sup>20,21)</sup>

In this review article, we shall give an overview of the results of ARPES studies dealing with the issue of the two gaps *versus* one gap. This article is written as follows: First, we demonstrate the material- and doping-dependence of the energy gaps. Next, we describe the temperature dependence of the energy gaps. Finally, we discuss the relationship between the observed energy gaps and  $T_c$ 's based on the Fermi arc picture.<sup>22,23)</sup>

## 2. Material and Doping Dependences of the Energy Gap

It has been well known that  $T_c$  in the optimally doped region ( $T_{c,\max}$ ) generally increases with the number ( $n$ ) of adjacent  $\text{CuO}_2$  planes from single layer ( $n = 1$ ), double layer ( $n = 2$ ), to triple layer ( $n = 3$ ). However, it has been unclear what governs the  $n$  dependence of  $T_{c,\max}$ . In this section, we shall explain the energy gap of the single layer, double layer, and triple layer cuprates, focusing on the deviation of the gap function in the antinodal region from the simple  $d$ -wave form.

First, we present the observation of the energy gap in the single-layer high- $T_c$  cuprates  $\text{La}_{2-x}\text{Sr}_x\text{CuO}_4$  (LSCO) to define the two energy scales. In Fig. 2, we show the result of ARPES studies of LSCO by Yoshida *et al.*<sup>17)</sup> Panels (a)-(c) show spectral weight mapping at  $E_F$  taken at  $T=20$  K for each doping level and clearly illustrate the intensity suppression in the anti-node region due to the gap being maximum there. Panels (d)-(f) show that the leading edge midpoints (LEMs) of energy distribution curves (EDCs) at the Fermi momenta  $k_F$  shift toward higher binding energies in going from the node to the anti-node, indicating an anisotropic low-temperature gap. The angular dependence of the gap for each doping is plotted as a function of the  $d$ -wave order parameter  $|\cos(k_x a) - \cos(k_y a)|/2$  in Fig. 3(a). Near the node (near  $|\cos(k_x a) - \cos(k_y a)|/2 \sim 0$ ), this plot obeys a straight line expected for the simple  $d$ -wave order parameter, but it starts to deviate upward around  $|\cos(k_x a) - \cos(k_y a)|/2 \sim 0.7$ - $0.9$ . Nearly the same results have been obtained for the optimally doped single-layer cuprates  $\text{Bi2201}$ .<sup>15,24)</sup> In order to characterize these behaviors of the energy gaps, one can define two energy scale parameters  $\Delta^*$  and  $\Delta_0$ :  $\Delta^*$  is a gap closest to  $|\cos(k_x a) - \cos(k_y a)|/2 = 1$  and  $\Delta_0$  is the extrapolated value of the linear simple  $d$ -wave gap near the node to  $|\cos(k_x a) - \cos(k_y a)|/2 = 1$ , as indicated in Fig. 1 and Fig. 3(a). In Fig. 3(b), the doping dependences of the  $\Delta^*$  and  $\Delta_0$  values thus deduced are plotted. The doping dependence of  $\Delta^*$  is consistent with various spectroscopic data such as tunneling and  $B_{1g}$ -symmetry Raman scattering.<sup>13)</sup>  $\Delta^* \sim 30$  meV for the  $x=0.15$  sample is consistent with the other ARPES results of single layer cuprates, too.<sup>15,18)</sup> On the other hand,  $\Delta_0$  remains unchanged in going from  $x=0.15$  to  $x=0.07$ , also the same as the result of  $\text{Bi2201}$ ,<sup>24)</sup> indicating a behavior contrasted with  $\Delta^*$ .

Next, let us look at the energy gaps of bi-layer materials which have much higher  $T_c$ 's than the single layer materials. Energy gaps at 10K observed by ARPES for underdoped  $\text{Bi2212}$  are presented in Fig. 4.<sup>14,25)</sup> As shown in Fig. 4(a), deviation from a simple  $d$ -wave form, becomes prominent with decreasing hole concentration, which is the same trend as the single layer cuprates as described above. On the other hand, one can find that the gap function of slightly underdoped  $\text{Bi2212}$  with  $T_c = 92$  K does not show a clear deviation from the simple

$d$ -wave form. This is contrasted with the case of the single layer cuprates, where the deviation from the simple  $d$ -wave is prominent not only in the underdoped but also in the optimally doped samples (Fig. 3). This difference stems from the much larger size of the near-nodal gap  $\Delta_0$  in Bi2212 than those of the single layer cuprates, making the condition  $\Delta^* > \Delta_0$  difficult to study. Another interesting point in Fig.4(a) is that the gap functions for various doping levels near the nodal direction are almost the same irrespective of the different  $T_c$ 's. In the same manner as in Fig. 3, the extracted  $\Delta^*$  and  $\Delta_0$  values of Bi2212 are plotted as functions of doping in Fig. 4(b).  $\Delta_0$  is nearly independent of the hole concentration from the optimal to underdoped regions, in contrast with the anti-nodal gap  $\Delta^*$  which increases with decreasing doping. Thus, not only  $\Delta^*$  but also  $\Delta_0$  do not trace the superconducting dome and, therefore, the relationship between the gaps and the  $T_c$  cannot be understood from the simple mean-field picture.

In the case of the tri-layer cuprate  $\text{Bi}_2\text{Sr}_2\text{Ca}_2\text{Cu}_3\text{O}_{10+\delta}$  (Bi2223), which has the highest  $T_{c,max}$  (=110 K) among the Bi-family cuprates, energy bands and Fermi surfaces originating from the outer and inner  $\text{CuO}_2$  planes (OP and IP) have been observed by Ideta *et al.*<sup>26)</sup> The hole concentration for the OP and IP bands deduced from the Fermi surface areas are 23% and 7%, respectively. Hence, the average hole concentration is 18%, close to the optimal doping concentration  $\sim 16\%$ . One may think that the deduced hole concentrations are influenced by the hybridization between the orbitals in neighboring  $\text{CuO}_2$  layers. However, the inter-layer hopping is small because the two OP bands do not show clear splitting. Hence, the effects of the hybridization on the estimated values would be negligible. In Figs. 5(a1)-(a3), we show the dispersions of the OP and IP bands in the superconducting state from the nodal to off-nodal cuts.<sup>26)</sup> The gap energies for both bands are very different, as in the case of other multi-layer cuprate  $\text{Ba}_2\text{Ca}_3\text{Cu}_4\text{O}_8\text{F}_2$  (F0234) with  $n = 4$ .<sup>27)</sup> The momentum dependence of the gap magnitude for OP is almost a simple  $d$ -wave,  $\Delta_0|\cos(k_x a) - \cos(k_y a)|/2$  with  $\Delta_0 \sim 43$  meV, as shown by a straight line in Fig. 5(b). The earlier ARPES results of Bi2223, where no clear band splitting has been observed, give the gap value of  $\sim 40$  meV, possibly reflecting the gap of the OP band.<sup>28-30)</sup> On the other hand, the gap for the IP band strongly deviates from the simple  $d$ -wave around the anti-node  $\sim (\pi, 0)$ . The gap size is therefore characterized by the two parameters  $\Delta_0 \sim 60$  meV around the node and  $\Delta^* \sim 80$  meV in the anti-nodal region. Because the deviation of the gap anisotropy from the simple  $d$ -wave is prominent in the underdoped cuprates, the observed gap anisotropy of the OP and IP are consistent with the doping levels of the OP and IP estimated from the FS areas. These energy gaps are much larger than those for the same doping level of the double-layer cuprates, which leads to the

higher  $T_c$  of Bi2223. Possible origins of the large superconducting gaps for the OP and IP is the minimal influence of out-of-plane disorder<sup>31)</sup> and/or interlayer tunneling of Cooper pairs between the OP and IP.<sup>32)</sup>

Now, let us compare the two gap energy scales for various kinds of high- $T_c$  cuprates. In Fig. 6, the doping dependences of  $\Delta^*$  and  $\Delta_0$  for the single-layer, double-layer and tri-layer cuprates are plotted. Interestingly, the doping dependence of the  $\Delta^*$  of all these samples approximately scale with the doping dependence of  $T^*$  estimated using various experimental techniques including ARPES as  $2\Delta^*/k_B T^* \simeq 4$ . Furthermore, in the underdoped region, the doping dependences of the value of  $\Delta^*$  and  $T^*$  are similar for all the systems irrespective of the very different  $T_{c,max}$ .<sup>17)</sup> Judging from the underdoped data, one can infer that  $\Delta^*$  is a universal property of a single  $\text{CuO}_2$  plane and is not strongly affected by interaction between layers.

One possible explanation for the material independence of  $\Delta^*$  is that its magnitude is determined by the exchange interaction  $J$ , since  $J$  is almost material independent. A pseudogap originating from antiferromagnetic spin fluctuations<sup>6,7)</sup> or RVB-type spin singlet formation<sup>33)</sup> has its origin in  $J$ . Indeed, a phenomenological model where the pseudogap  $\Delta^*$  comes from the RVB gap explains the two characteristic gap energy scales.<sup>34,35)</sup> We should also note that, as discussed in the next section, the behavior of the anti-nodal gap  $\Delta^*$  is consistent with a density-wave order model<sup>36)</sup> and may be relative to the nanoscale inhomogeneity observed by STM.<sup>4)</sup>

In contrast to the nearly material-independent  $\Delta^*$ , the nodal  $d$ -wave order parameter  $\Delta_0$  of the optimally doped Bi2212 is twice as large as those of LSCO and Bi2201. Furthermore, Bi2223 has even larger  $\Delta_0$ 's than Bi2212 as shown in Fig.6(c). These material dependence roughly follows the magnitude of maximum  $T_c$ . The strong material dependences of  $\Delta_0$  imply that  $\Delta_0$  is not only a property of a single  $\text{CuO}_2$  plane but also a property influenced by the apical oxygens, the block layers and/or the neighboring  $\text{CuO}_2$  planes. Namely, the number of  $\text{CuO}_2$  layers and/or the distance of the apical oxygen atoms (in the block layers) from the  $\text{CuO}_2$  plane might be important factors for determining the  $\Delta_0$  and hence  $T_{c,max}$ . Influence from outside the  $\text{CuO}_2$  plane has been modelled using the distant-neighbor hopping parameters,  $t'$  and  $t''$ ,<sup>37)</sup> which are affected by the  $p_z$  orbital of the apical oxygen, the nearly filled Cu  $3d_{z^2}$  orbital, and the position of the empty Cu  $4s$  orbital.

### 3. Temperature Dependence of the Energy Gaps and the Fermi Arc

In the preceding section, we have demonstrated distinct doping dependence of the near-nodal and near-antinodal gaps, as well as a ubiquitous deviation from the simple  $d$ -wave form in underdoped samples. This is because the superconducting gap and the pseudogap may dominate in the nodal and antinodal regions, respectively. The different natures of the pseudogap and the superconductivity are also evident in their material dependences. In this section, we further emphasize their distinct behaviors via temperature dependent studies in different momentum regions. We discuss the interplay between the pseudogap and the superconductivity, and possible microscopic origins of the pseudogap.

Figure 7(a) shows the temperature dependence of the gap in Bi2212 reported by Lee *et al.*<sup>25)</sup> At low temperatures, the symmetrized EDC's [panel (c)] on the Fermi surface near the node show two peaks above and below  $E_F$ . They shift towards each other with increasing temperature, indicating a gradual closing of the gap, and eventually merge into a single peak at  $E_F$  above  $T_c$ , indicating the disappearance of the gap. Correspondingly, the peak above  $E_F$  in the raw spectra [panel (a)], which can be understood as the upper branch of the Bogoliubov quasi-particle, moves closer to  $E_F$  with temperature and disappears above  $T_c$  [panels (a) and (b)]. Note that the peaks abruptly disappear above  $T_c$ , which cannot be explained by trivial thermal broadening. In panel (e), the temperature dependences of the gap size for several cuts evaluated from the symmetrized EDC's are summarized. The near-nodal gap closes at  $\sim T_c$ , reminiscent of the BCS theory, although the exact functional form may be different. This indicates that the gap near the node is primarily of the superconductivity origin.

The lowest binding energy peak in the antinodal region, on the other hand, does not show a strong temperature dependence across  $T_c$ , from the underdoped to the overdoped samples, as shown in Fig. 7(d). Interestingly, without closing the gap, the sharp superconducting QP peak almost disappears above  $T_c$ .<sup>25,38)</sup> The intensity of the QP peak below  $T_c$  scales with the superfluid density and the condensation energy.<sup>38)</sup> This suggests that the temperature dependences of the gap magnitude and the spectral intensity in the antinodal region does not follow the weak-coupling BCS theory. Therefore, it is difficult to explain these two different types of temperature dependences in the different momentum regions of a single Fermi surface using a single order parameter. The existence of multiple order parameters is hence implied, and this further emphasizes the two-gap behavior and the nodal-antinodal dichotomy. Here, it should be noted that the dichotomous temperature dependence is not a sharp dichotomy in momentum space, but rather a crossover from the temperature dependence near the node to the temperature independence near the antinode. In fact, the temperature dependence in the

intermediate momentum region shows intermediate behaviors: the gap becomes smaller but does not close completely above  $T_c$ . Moreover, at the lowest temperature even the slightly underdoped Bi2212 (UD92K) shows nearly the simple  $d$ -wave form, despite that the temperature dependences near the node and antinode are completely different as described above. Here, it should be noted that we also observe a superconducting QP peak even in the anti-nodal region well below  $T_c$ .<sup>25,39)</sup> This suggests that contribution to the condensation energy from the anti-nodal electronic states is finite even though it is weakened by the pseudogap opening. It seems natural to consider that the superconducting gap near the antinode is strongly distorted by the pseudogap, leading to the deviation of the gap function and the coherent QP intensity from the simple  $d$ -wave functional form.

Because of the nodal-antinodal dichotomy in the temperature dependence of the gap, as shown in Fig.7, slightly above  $T_c$ , only a portion of the Fermi surface is recovered near the node. We refer to this ungapped portion of the Fermi surface above  $T_c$  as the ‘‘Fermi arc’’. Here, we define the Fermi arc by the momentum region where symmetrized EDCs at  $k_F$  have a single peak at  $E_F$  at each temperature above  $T_c$ . It thus looks as if the original hole-like Fermi surface is truncated into four pieces in the first Brillouin zone, although there are still debates whether the ungapped portion is actually part of the original Fermi surface or part of small hole pockets.<sup>6,40,41)</sup> The Fermi arc length seems proportional to the hole concentration and is shown to increase with temperature.<sup>42)</sup> As shown below, the Fermi arc length slightly above  $T_c$  will be used in the analysis between energy gap and  $T_c$ .

In Fig. 8, we show another case of the temperature dependence of the gap, namely, tri-layer cuprates Bi2223 reported by Ideta *et al.*<sup>43)</sup> As in the case of Bi2212, the gap near the node has the simple  $d$ -wave form and closes just above  $T_c$  to form a Fermi arc, again suggesting the major contribution of the nodal region to the superconductivity. The gap function of the (underdoped) IP clearly shows the two-gap behavior well below  $T_c$ , and the Fermi arc length slightly above  $T_c$  is shorter than that for the OP, reflecting the lower hole concentration of the IP. The gap in the antinodal region of the (overdoped) OP remains open already above  $T_c$  with little temperature dependence, although the gap function well below  $T_c$  follows the  $d$ -wave form. A QP peak exists on the entire Fermi surface similar to the Bi2212 case. Similar behaviors have also been reported in the single-layer cuprate families.<sup>15,24,44,45)</sup> These observation lead the conclusion that the nodal-antinodal dichotomy and the existence of the Fermi arc are the universal features of the cuprate. The almost BCS-like temperature dependence of the gap on the Fermi arc suggests that the Fermi arc is closely related to the superconductivity.

Focusing on the detailed temperature dependence of the antinodal pseudogap of the single-layer Bi2201, Hashimoto *et al.* have shown that the antinodal gap is not caused by superconductivity but it is more consistent with a short-range density-wave order by studying the gap energy and the entire band dispersion.<sup>36,46)</sup> Since the  $T_c$  ( $\sim 34$  K) of this system is low and the difference between  $T^*$  ( $\sim 125$  K) and  $T_c$  is relatively large, one can study the pseudogap state between  $T_c$  and  $T^*$  in great detail. As one can see from Figs. 9(b) and (c), above  $T^*$ , the ARPES spectra along an antinodal cut [inset of Fig. 9(c)] show a parabolic dispersion crossing  $E_F$ . This is strikingly simple, like the dispersion in a simple metal, and we define  $k_F$  unambiguously from the Fermi crossing points. Note that, since the superconducting peak is very weak in this compound, the pseudogap dispersion can be studied below  $T_c$ . The pseudogap opens at  $T < T^*$ , and spectra at these lower temperatures are paradoxically broader than at higher temperature. We track the dispersion by the peak positions of EDCs at different  $k$  points. In the 10 K spectra displayed in Fig. 9(d), no “back-bending” is observed at  $k_F$  defined above  $T^*$ . Instead, the dispersion bends back at momenta markedly away from the  $k_F$ . Very importantly, this misalignment of the back-bending momentum and  $k_F$  cannot be explained by the opening of a simple superconducting gap, which requires a gap with particle-hole symmetry. As shown in Fig. 9(a), one always expects the alignment of  $k_F$  and the “back-bending” momentum of the dispersion in the superconducting state. Because of this strong constraint, it can be concluded that the observed behavior below  $T^*$  is different from the expectation for the superconducting state, suggesting that the transition from the true normal state above  $T^*$  to the pseudogap state has a different origin from Cooper pairing. The smooth temperature evolution upon cooling from the true normal state<sup>36)</sup> suggests a direct connection of the broken-symmetry state below  $T^*$  with the pseudogap opening. Also, the temperature dependence of the antinodal gap in the ARPES spectra coincides with the results of polar Kerr rotation and time-resolved reflectivity.<sup>46)</sup> This particle-hole asymmetric gap may be explained by some sort of density wave order with short correlation length. It is found that the simulations of both the checkerboard density-wave order of orthogonal wave vectors and commensurate  $(\pi, \pi)$  density-wave order can qualitatively reproduce the misalignment of the back-bending momentum and  $k_F$  and the stronger dispersion at lower temperatures. The anomalous broadening upon pseudogap opening could be understood if finite correlation length of the density wave order is considered.<sup>36,46)</sup> Intriguingly, the density wave order considered here could be consistent with the momentum-integrated STM observations in real space.<sup>5)</sup> Furthermore, broken spatial symmetry with nematic order and its finite correlation length have been reported in the pseudogap phase.<sup>47)</sup> The observed nanoscale inhomogeneity



associated with local density-wave order is formally consistent with the spatially-averaged observation by ARPES, and supports that the pseudogap is a broken-symmetry state below  $T^*$ . This pseudogap most likely competes with superconductivity, leaving the form of the interaction between the pseudogap and superconductivity as an open question.

Now, we turn to the subject of scaling relationship related  $T_c$  in the high- $T_c$  cuprates. The well known Uemura relationship relates the superfluid density with  $T_c$ <sup>48)</sup> for underdoped cuprates. Tallon *et al.*<sup>49)</sup> have proposed a modified Uemura relation in which the value of  $T_c/\Delta'$  plotted as a function of superfluid density, where  $\Delta'$  is the maximum spectral gap obtained from the specific heat and Raman studies. Since an energy gap presumably due to competing order is open already above  $T_c$ , one may infer that the pseudogap weakens contribution to the condensation energy from the anti-nodal region as indicated by the superconducting peak ratio.<sup>38)</sup> Then, we propose another relationship between the Fermi arc and  $T_c$ . Here, we define the “effective” superconducting gap  $\Delta_{sc}$ , by the gap at the end point of the Fermi arc slightly above  $T_c$ , [ $\propto$ (Fermi arc length)  $\times \Delta_0$ ]. Then,  $\Delta_{sc}$  rather than  $\Delta_0$  would be more directly related to  $T_c$ .<sup>22)</sup> Note that this is a  $T = T_c$  scaling relation rather than a  $T = 0$  scaling relation like the Uemura relation.

In Fig. 10(a), we plot the nodal superconducting gap  $\Delta_0$  measured by ARPES (Fig. 6) *versus*  $T_c$  for various high- $T_c$  cuprates. For optimally-doped to overdoped samples, the experimental data follow the relationship  $2\Delta_0 \sim 9k_B T_c$ , reminiscent of a strong coupling formula of  $d$ -wave superconductivity, and in the underdoped region, the plot becomes  $2\Delta_0 \gg 9k_B T_c$ , deviating from the linear relationship between  $\Delta_0$  and  $T_c$ . Next, we apply our scaling analysis with the Fermi arc length  $K_a$ . In Fig. 10(b),  $K_a$  for LSCO,<sup>17,18)</sup> Bi2201,<sup>15)</sup> Bi2212,<sup>25,42)</sup> and the OP and IP of Bi2223<sup>43)</sup> are plotted as a function of doped hole concentration  $x$ . One finds that the  $K_a$  values of the various high- $T_c$  cuprates approximately fall on a single line. Here, we should note that the magnitude of the antinodal gap  $\Delta^*$  in the underdoped region, which is nearly material independent, may have an inverse correlation with  $K_a$ , which may cause a material independence of  $K_a$ . The evolution of  $K_a$  with  $x$  implies increase of holes in the normal state. Tanner *et al.*<sup>50)</sup> pointed out that the number of superconducting electrons  $n_s$  is empirically proportional to the number of normal state carrier  $n_n$ :  $n_s \sim 0.2n_n$ . Therefore, the Fermi arc length also scales with superfluid density  $\rho_s = n_s/m^*$ ,<sup>24)</sup> where  $m^*$  is the carrier effective mass.

In Fig. 10(c), we have plotted the “effective” superconducting gap  $\Delta_{sc} = \Delta_0 \sin(K_a/k_F)$  against  $T_c$  for various high- $T_c$  cuprates. These data approximately fall on the straight dotted line ( $2\Delta = 4k_B T_c$ ) which is close to the  $d$ -wave BCS gap ratio  $2\Delta_{\text{BCS}} = 4.3k_B T_c$ .<sup>51)</sup> It

should be noted that this relationship seems to hold even in the overdoped region. Hence, the “effective” superconducting gap  $\Delta_{sc} \propto K_a \Delta_0$  scales with  $T_c$  better than  $\Delta_0$  does. This relationship is reminiscent of the relationship  $T_c \propto x \Delta_0$  proposed by Lee and Wen<sup>23)</sup> and Oda *et al.*<sup>22)</sup> The closer relationship between  $\Delta_{sc}$  and  $T_c$  than that between  $\Delta_0$  and  $T_c$  implies that contribution to the condensation of superfluid from the anti-nodal region may be reduced due to the gap opening above  $T_c$ . While the relationship between  $\Delta_{sc}$  and  $T_c$  is close to the weak-coupling BCS formula  $2\Delta_{BCS} \simeq 4.3k_B T_c$  [Fig. 10(c)],  $\Delta_0$  satisfies the strong-coupling relationship  $2\Delta_0 \simeq 9k_B T_c$  [Fig. 10(a)] from the optimum to the overdoped regions. When the gap has a simple  $d$ -wave form in the overdoped samples,  $\Delta_0$  may be comparable or larger than the magnitude of the gap from competing order. How the competing order fades away with doping in the overdoped region is an open question to be addressed in future studies.

#### 4. Conclusion

We have presented an overview of the two-gap behaviors in the high- $T_c$  cuprates observed by ARPES and described the doping, material, and temperature dependences of the energy gaps. Two distinct energy scales  $\Delta^*$  and  $\Delta_0$  have been identified to describe the two-gap energy structure where their momentum dependence sometime deviates from the simple  $d$ -wave. The observed energy gaps show dichotomy between the near nodal (characterized by  $\Delta_0$ ) and anti-nodal direction (characterized by  $\Delta^*$ ) regions. While  $\Delta^*$  at the same doping level is nearly material independent,  $\Delta_0$  shows a strong material dependence reflecting the magnitude of  $T_{c,\max}$ . As for the temperature dependence, the gap near the nodal direction closes at  $T_c$ . In contrast, the anti-nodal gap does not close at  $T_c$  and its spectral features cannot be explained by conventional superconductivity, but consistent with a short-range density-wave picture.<sup>36)</sup> Therefore, the origin of  $\Delta^*$  is likely to be a density-wave order competing with the superconductivity, although finite contribution of the pseudogapped region to the superconductivity may also exist. From  $\Delta_0$  and the Fermi arc length,  $K_a$ , we define an “effective superconducting gap”  $\Delta_{sc}$ , which scales with  $T_c$  through  $2\Delta_{sc} \simeq 4k_B T_c$ , though this relationship does not imply that superconductivity is absent away from the Fermi arc below  $T_c$ . The results give a reasonable scaling with  $T_c$  for different materials. To fully elucidate the two-gap behavior, both phenomena, the competing order and the superconducting fluctuations, should be properly taken into account. This issue should be clarified in future studies of the electronic structure by ARPES and STM.

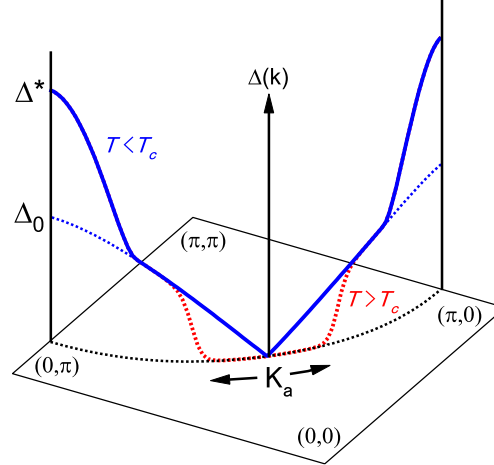


Fig. 1. (Color online) Schematic picture of the energy gap on the Fermi surface of the high- $T_c$  cuprate superconductor. Deviation of the energy gap from the simple  $d$ -wave is characterized by the  $d$ -wave-like nodal gap ( $\Delta_0$ ) and the larger anti-nodal gap ( $\Delta^*$ ). Above  $T_c$ , the gap in the nodal direction closes. The Fermi arc length  $K_a$  is defined by the zero gap region on the Fermi surface slightly above  $T_c$ . The gap becomes simple  $d$ -wave-like when  $\Delta^*$  becomes as small as  $\Delta_0$ .

### Acknowledgement

This work was supported by a Grant-in-Aid for Young Scientist B (22740221), the A3 Foresight Program from the Japan Society for the Promotion of Science, and by DOE Office of Basic Energy Science, Division of Materials Science (Contract number DE-FG03-01ER45929-A001 and DE-AC02-76SF00515)

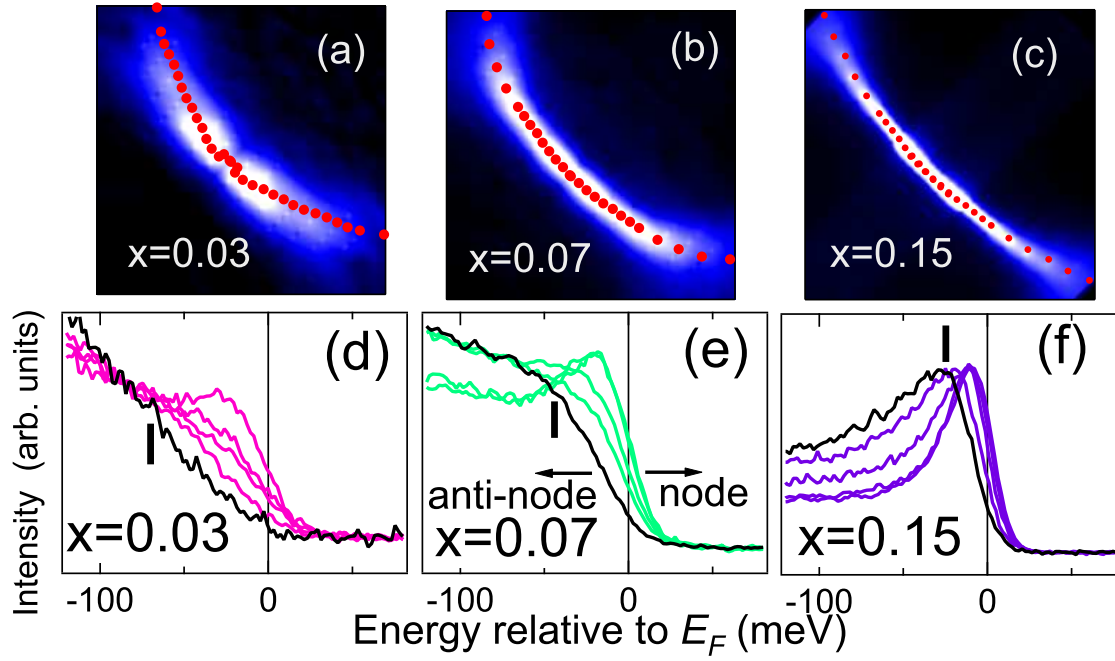


Fig. 2. (Color online) Fermi surface and energy distribution curves (EDCs) at  $k_F$  in  $\text{La}_{2-x}\text{Sr}_x\text{CuO}_4$  (LSCO) with various doping levels taken at  $T=20\text{ K}$ .<sup>17)</sup> (a)-(c): Spectral weight mapping at  $E_F$  in momentum space for each doping level. Red dots indicate Fermi momenta  $k_F$  defined by the peak positions of the momentum distribution curves. (d)-(f): EDCs at  $k_F$  for each doping level. Black lines correspond to antinodal EDCs and vertical bars represent energy position of the antinodal gap.

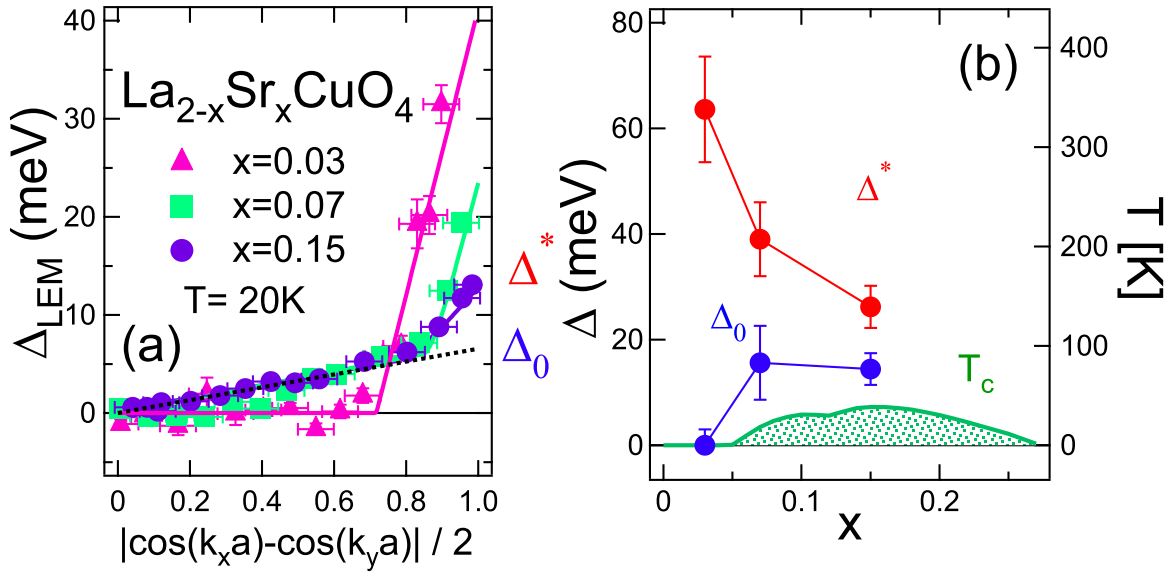


Fig. 3. (Color online) Momentum dependence of the energy gap at  $T=20\text{K}$  in  $\text{La}_{2-x}\text{Sr}_x\text{CuO}_4$  with various doping levels.<sup>17)</sup> (a): Leading edge midpoints (LEM)  $\Delta_{\text{LEM}}$  relative to that at the node. (b): Doping dependence of  $\Delta^*$  and  $\Delta_0$  obtained by assuming the relationship  $\Delta_{\text{peak}} \simeq 2.2\Delta_{\text{LEM}}$ .

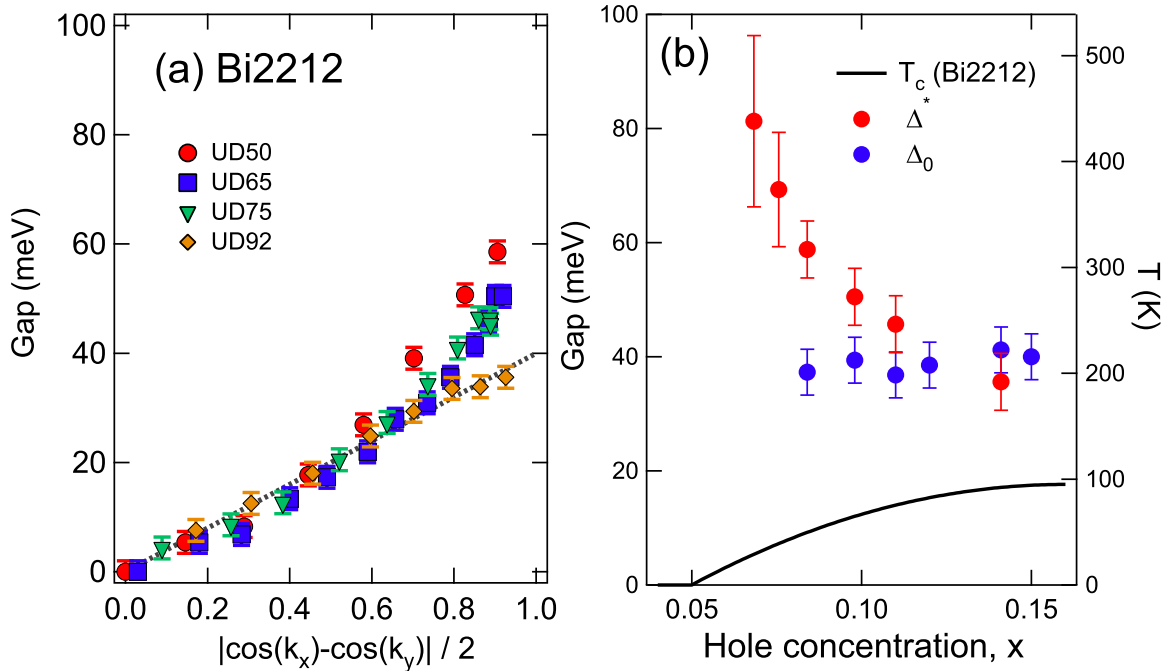


Fig. 4. (Color online) Energy gaps for underdoped Bi2212. (a) Momentum dependence of the energy gap measured at  $10\text{K}$ .<sup>14,25)</sup> A deviation from a simple  $d$ -wave form (dashed line) is observed near the antinode in underdoped samples with  $T_c < 92\text{K}$ . (b) Doping dependences of the nodal gap  $\Delta_0$  and the anti-nodal gap  $\Delta^*$ . The  $T_c$  dome of Bi2212 is also plotted.

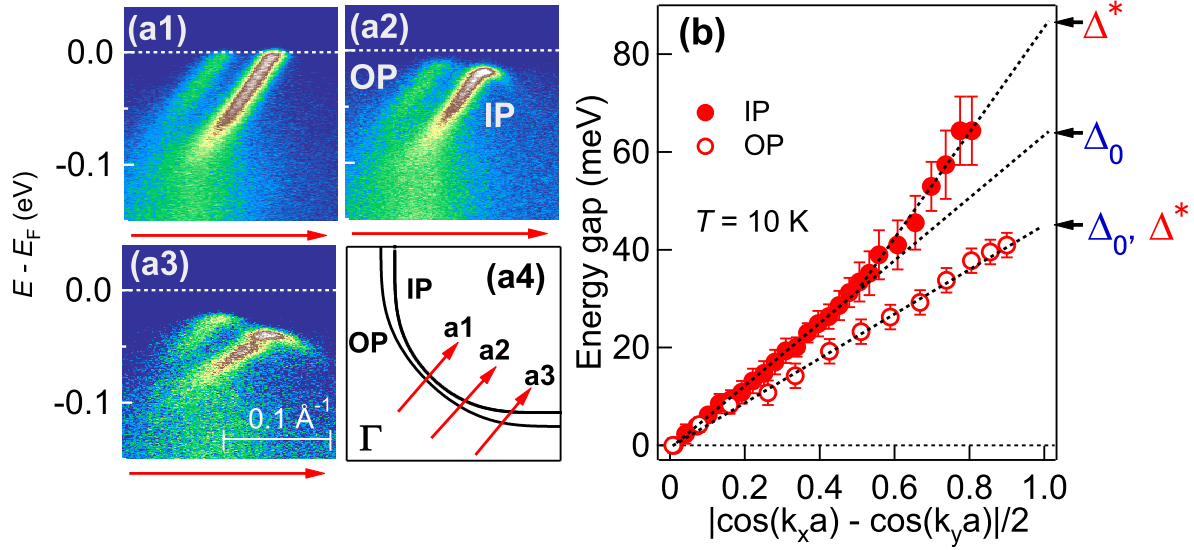


Fig. 5. (Color online) Energy gap in the superconducting state ( $T=10\text{K}$ ) of optimally doped Bi2223.<sup>26)</sup> (a1)-(a3) Energy-momentum intensity plots of the cuts from the nodal to off-nodal regions for the outer and inner CuO<sub>2</sub> plane (OP and IP) bands. The corresponding cuts are shown in panel (a4). These data were taken with a photon energy of  $h\nu=11.95 \text{ eV}$ . (b) Momentum dependences of the energy gaps for the OP and IP bands. The definition of the nodal gap  $\Delta_0$  and the antinodal gap  $\Delta^*$  is shown.

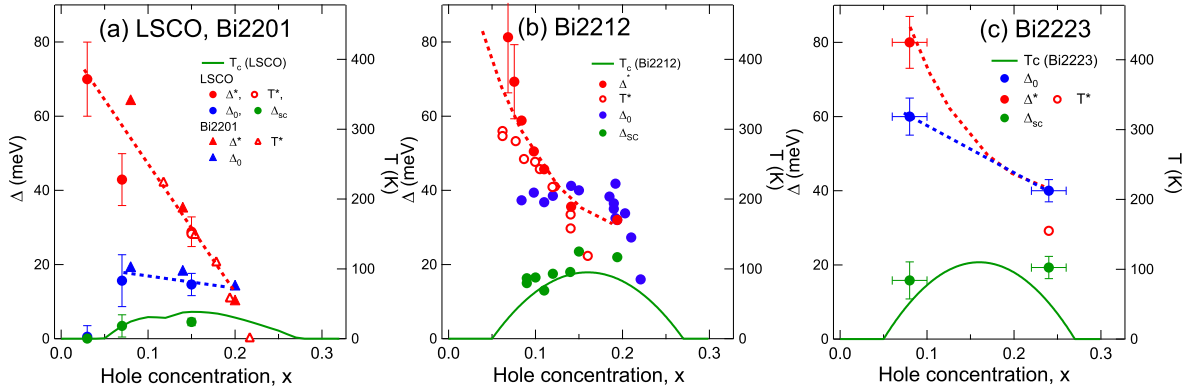


Fig. 6. (Color online) Doping dependences of the characteristic energies ( $\Delta^*$ ,  $\Delta_0$ ) and temperatures ( $T^*$ ,  $T_c$ ) for the single-layer cuprates (LSCO, Bi2201) (a), the double-layer cuprates Bi2212 (b) and the tri-layer cuprates Bi2223 (c). Gap energies  $\Delta$  and temperatures  $T$  have been scaled as  $2\Delta = 4.3k_B T$  in these plots. Parameter values have been taken from the ARPES studies of LSCO,<sup>17,18)</sup> Bi2201,<sup>24)</sup> Bi2212<sup>8,14,25,52,53)</sup> and Bi2223.<sup>26,28)</sup>  $T^*$  for Bi2201 and Bi2212 have been taken from the NMR<sup>20)</sup> and the transport studies,<sup>54)</sup> respectively.  $\Delta_{sc}$  defined in the text approximately follows the  $T_c$  dome. Dashed curves are guide to the eye for  $\Delta^*$  and  $\Delta_0$ .

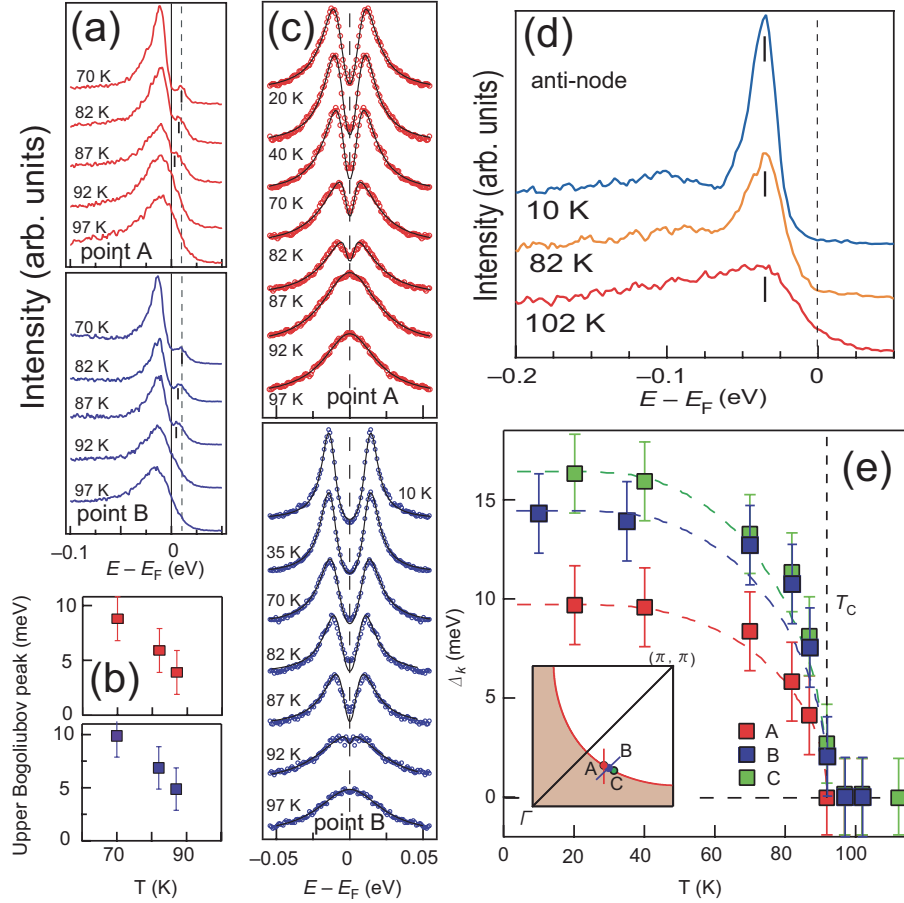


Fig. 7. (Color online) Temperature dependence of the gap in Bi2212<sup>25)</sup> (a) Temperature dependences of the raw spectra at different  $k_F$ 's near the node across  $T_c$  in underdoped Bi2212 ( $T_c = 92$  K,  $p \sim 0.14$ ) at point A (upper panel) and B (lower panel). The upper Bogoliubov peaks are indicated by bars. (b) Temperature dependence of the energy position of upper Bogoliubov peaks. (c) Symmetrized EDCs across  $T_c$  at point A (upper panel) and B (lower panel). (d) Temperature dependence of the EDC at the antinode on the Brillouin zone boundary across  $T_c$ . Peak positions are indicated by bars. (e) Fitted gap size as a function of temperature at different near-nodal momenta, showing the BCS-like gap closing.

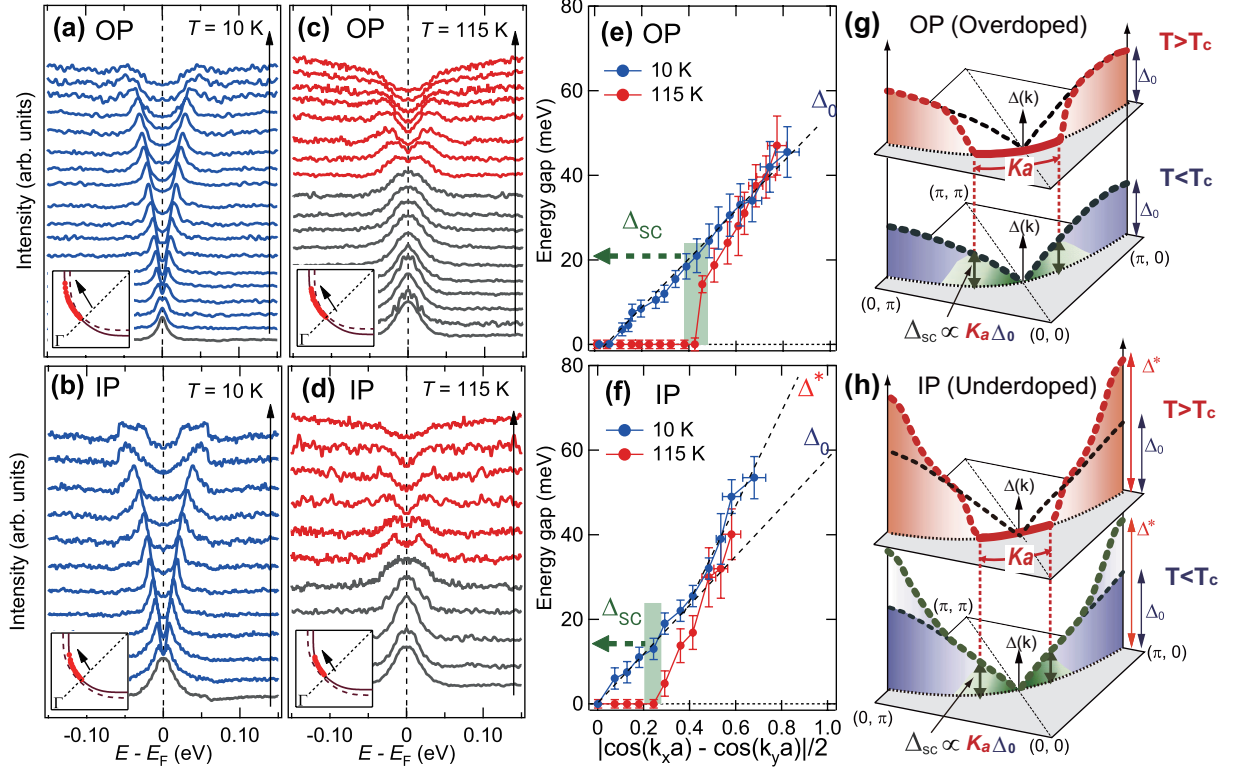


Fig. 8. (Color online) Momentum dependence of the energy gap along the Fermi surface at  $T \ll T_c$  and  $T > T_c$  in optimally doped Bi2223 ( $T_c = 110$  K).<sup>43)</sup> (a) Symmetrized EDCs along the outer plane (overdoped) Fermi surface at 10 K. (b) Symmetrized EDCs along the inner plane (underdoped) Fermi surface at 10 K. (c)(d) Symmetrized EDCs above  $T_c$  ( $T = 115$  K). (e)(f) Fitted gap size below and above  $T_c$  along the Fermi surfaces for the outer and inner planes (OP and IP), respectively. (g)(h) Schematic drawings of the evolution of the gap with temperature for the outer and inner planes, respectively. The Fermi arc length ( $K_a$ ),  $\Delta_0$ ,  $\Delta^*$  and effective superconducting gap  $\Delta_{sc}$  are defined.



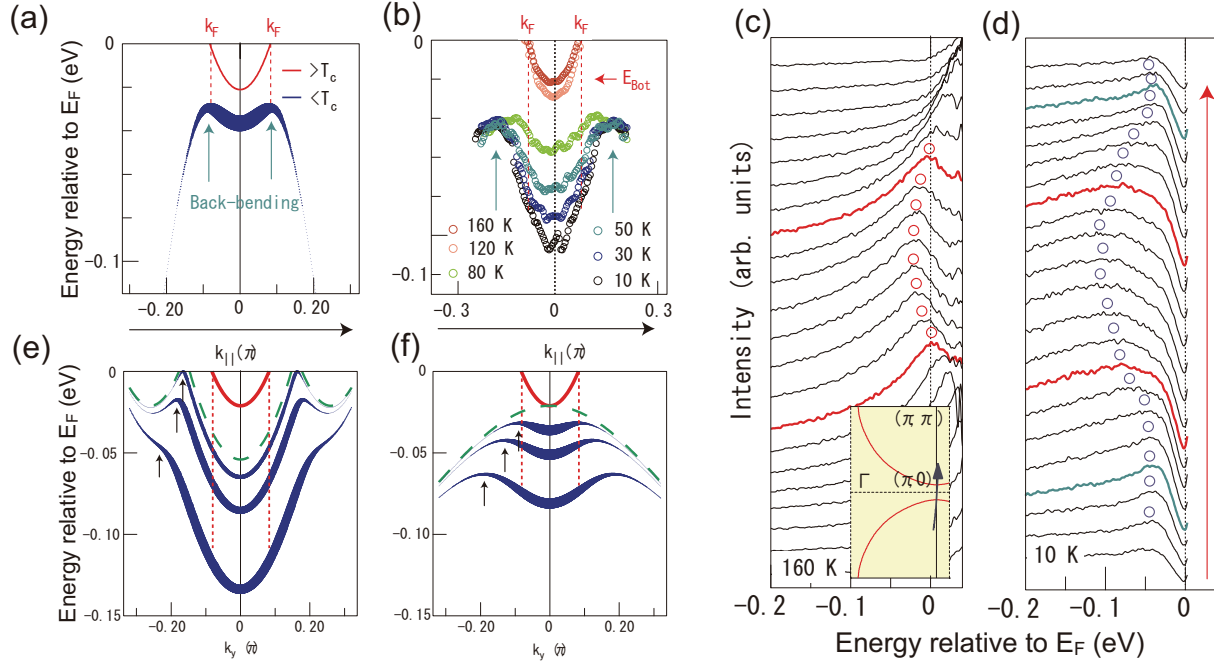


Fig. 9. (Color online) Particle-hole symmetry breaking in the antinodal pseudogapped dispersion of the single layer Bi2201. (a) Simulated dispersion for  $d$ -wave homogeneous superconductivity with order parameter  $V = 30$  meV along  $(-\pi, \pi) - (\pi, 0) - (\pi, \pi)$ . Note that the back-bending momentum is aligned to  $k_F$ . (b) Experimentally determined temperature evolution of the dispersion across  $T^* \sim 125$  K. (c) EDCs in the ungapped state above  $T^*$ . Inset shows the measured cut. (d) EDCs at 10 K. Red EDCs are for  $k_F$ . The dispersion shows no anomaly at  $k_F$ . (e)(f) Simulated dispersion for Two long-range orders: (e) incommensurate checkerboard density-wave order of orthogonal wave vectors,  $[0.26\pi, 0]$ ,  $[0, 0.26\pi]$  and (f) commensurate  $[\pi, \pi]$  density-wave order with order parameter  $V = 15, 30$  and  $60$  meV (from top to bottom). Back-bendings are indicated by arrows.

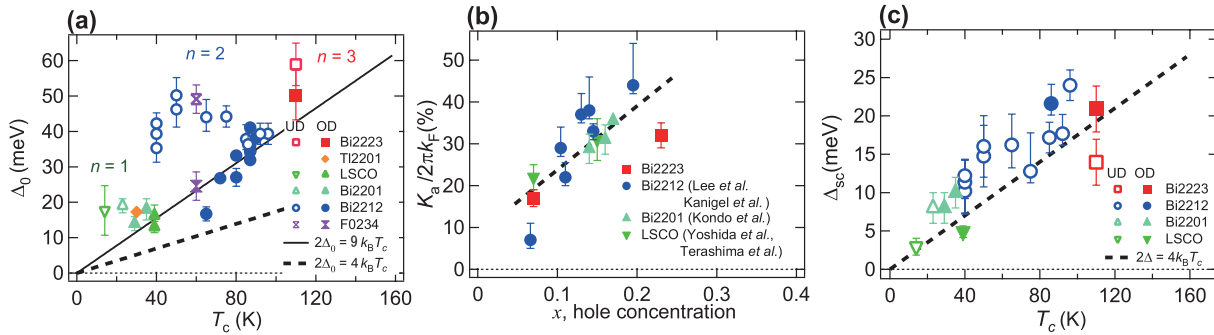


Fig. 10. (Color online) Relationship between the nodal superconducting gap  $\Delta_0$ , the Fermi arc length  $K_a$ , the superconducting gap at the edge of the Fermi arc  $\Delta_{sc}$  and  $T_c$  for various high- $T_c$  cuprates. (a)  $\Delta_0$  as a function of  $T_c$ . Data are taken from ARPES results for LSCO, Bi2201, Bi2212, Bi2223 in Fig.6 and F0234.<sup>27)</sup> (b)  $K_a$  relative to that of the full Fermi surface  $2\pi k_F$  as a function of hole concentrations. Dashed line is a guide to the eye. (c)  $\Delta_{sc}$  as a function of  $T_c$ . The dashed line indicates  $2\Delta = 4 k_B T_c$ , which is close to the weak coupling  $d$ -wave BCS relationship.

**References**

- 1) P. W. Anderson: *Science* **235** (1987) 1196.
- 2) J. V. Emery and S. A. Kivelson: *Nature* **374** (1998) 434.
- 3) S. Chakravarty, R. B. Laughlin, D. K. Morr, and C. Nayak: *Phys. Rev. B* **63** (2001) 094503.
- 4) T. Hanaguri, C. Lupien, Y. Kohsaka, D.-H. Lee, M. Azuma, M. Takano, H. Takagi, and J. C. Davis: *Nature* **430** (2004) 1001.
- 5) W. D. Wise, M. C. Boyer, K. Chatterjee, T. Kondo, T. Takeuchi, H. Ikuta, Y. Wang, and E. W. Hudson: *Nature Phys.* **4** (2008) 696.
- 6) H. Kamimura, T. Hamada, and H. Ushio: *Phys. Rev. B* **66** (2002) 054504.
- 7) P. Prelovsek and A. Ramsak: *Phys. Rev. B* **65** (2002) 174529.
- 8) J. C. Campuzano, H. Ding, M. R. Norman, H. M. Fretwell, M. Randeria, A. Kaminski, J. Mesot, T. Takeuchi, T. Sato, T. Yokoya, T. Takahashi, T. Mochiku, K. Kadowaki, P. Guptasarma, D. G. Hinks, Z. Konstantinovic, Z. Z. Li, , and H. Raffy: *Phys. Rev. Lett.* **83** (1999) 3709.
- 9) N. Miyakawa, P. Guptasarma, J. F. Zasadzinski, D. G. Hinks, and K. E. Gray: *Phys. Rev. Lett.* **80** (1998) 157.
- 10) G. Deustercher: *Nature* **397** (1999) 410.
- 11) C. Panagopoulos, J. R. Cooper, and T. Xiang: *Phys. Rev. B* **57** (1998) 13422.
- 12) M. Opel, R. Nemeschek, C. Hoffmann, R. Philipp, P. F. Müller, R. Hackl, I. Tüttö, A. Erb, B. Revaz, E. Walker, H. Berger, and L. Forró: *Phys. Rev. B* **61** (2000) 9752.
- 13) M. L. Tacon, A. Sacuto, A. Georges, G. Kotliar, Y. Gallais, D. Colson, and A. Forget: *Nature Physics* **2** (2006) 537.
- 14) K. Tanaka, W. S. Lee, D. H. Lu, A. Fujimori, T. Fujii, Risdiana, I. Terasaki, D. J. Scalapino, T. P. Devereaux, Z. Hussain, and Z.-X. Shen: *Science* **314** (2006) 1910.
- 15) T. Kondo, T. Takeuchi, A. Kaminski, S. Tsuda, and S. Shin: *Phys. Rev. Lett.* **98** (2007) 267004.
- 16) M. Hashimoto, T. Yoshida, A. Fujimori, D. Lu, Z.-X. Shen, M. Kubota, K. Ono, M. Ishikado, K. Fujita, and S. Uchida: *Phys. Rev. B* **79** (2009) 144517.
- 17) T. Yoshida, M. Hashimoto, S. Ideta, A. Fujimori, K. Tanaka, N. Mannella, Z. Hussain, Z.-X. Shen, M. Kubota, K. Ono, S. Komiya, Y. Ando, H. Eisaki, and S. Uchida: *Phys. Rev. Lett.* **103** (2009) 037004.
- 18) K. Terashima, H. Matsui, T. Sato, T. Takahashi, M. Kofu, and K. Hirota: *Phys. Rev. Lett.* **99** (2007) 017003.
- 19) M. Hashimoto, T. Yoshida, K. Tanaka, A. Fujimori, M. Okusawa, S. Wakimoto, K. Yamada, T. Kakeshita, H. Eisaki, and S. Uchida: *Phys. Rev. B* **75** (2007) 140503(R).
- 20) G. q. Zheng, P. L. Kuhns, A. P. Reyes, B. Liang, and C. T. Lin: *Phys. Rev. Lett.* **94** (2005) 047006.
- 21) S. Kawasaki, C. Lin, P. L. Kuhns, A. P. Reyes, and G.-q. Zheng: *Phys. Rev. Lett.* **105** (2010) 137002.
- 22) M. Oda, R. M. Dipasupil, N. Momono, and M. Ido: *J. Phys. Soc. Jpn.* **69** (2000) 983.
- 23) P. A. Lee and X.-G. Wen: *Phys. Rev. Lett.* **78** (1997) 4111.
- 24) T. Kondo, R. Khasanov, T. Takeuchi, J. Schmalian, and A. Kaminski: *Nature* **457** (2009) 296.
- 25) W. S. Lee, I. M. Vishik, K. Tanaka, D. H. Lu, T. Sasagawa, N. Nagaosa, T. P. Devereaux, Z. Hussain, and Z.-X. Shen: *Nature* **450** (2007) 81.
- 26) S. Ideta, K. Takashima, M. Hashimoto, T. Yoshida, A. Fujimori, H. Anzai, T. Fujita,

- Y. Nakashima, A. Ino, M. Arita, H. Namatame, M. Taniguchi, K. Ono, M. Kubota, D. H. Lu, Z.-X. Shen, K. M. Kojima, and S. Uchida: *Phys. Rev. Lett.* **104** (2010) 227001.
- 27) Y. Chen, A. Iyo, W. Yang, X. Zhou, D. Lu, H. Eisaki, T. P. Devereaux, Z. Hussain, and Z.-X. Shen: *Phys. Rev. Lett.* **97** (2006) 236401.
- 28) T. Sato, H. Matsui, S. Nishina, T. Takahashi, T. Fujii, T. Watanabe, and A. Matsuda: *Phys. Rev. Lett.* **89** (2002) 067005.
- 29) T. Sato, H. Matsui, T. Takahashi, H. Ding, H.-B. Yang, S.-C. Wang, T. Fujii, T. Watanabe, A. Matsuda, T. Terashima, and K. Kadowaki: *Phys. Rev. Lett.* **91** (2003) 157003.
- 30) H. Matsui, T. Sato, T. Takahashi, H. Ding, H.-B. Yang, S.-C. Wang, T. Fujii, T. Watanabe, A. Matsuda, T. Terashima, and K. Kadowaki: *Phys. Rev. B* **67** (2003) 060501.
- 31) H. Eisaki, N. Kaneko, D. L. Feng, A. Damascelli, P. K. Mang, K. M. Shen, Z.-X. Shen, and M. Greven: *Phys. Rev. B* **69** (2004) 064512.
- 32) S. Chakravarty, H.-Y. Kee, and K. Völker: *Nature* **428** (2004) 53.
- 33) H. Fukuyama and H. Kohno: *ined. H. Fukuyama and N. Nagaosa* (Springer, Berlin, 1999), p. 231.
- 34) K. Y. Yang, T. M. Rice, and F. C. Zhang: *Phys. Rev. B* **73** (2006) 174501.
- 35) K. Y. Yang, H. B. Yang, P. D. Johnson, T. M. Rice, and F. C. Zhang: *Europhys. Lett.* **86** (2009) 37002.
- 36) M. Hashimoto, R.-H. He, K. Tanaka, J.-P. Testaud, W. Meevasana, R. G. Moore, D. Lu, H. Yao, Y. Yoshida, H. Eisaki, T. P. Devereaux, Z. Hussain, and Z.-X. Shen: *Nature Phys.* **6** (2010) 414.
- 37) E. Pavarini, I. Dasgupta, T. Saha-Dasgupta, O. Jepsen, and O. K. Andersen: *Phys. Rev. Lett.* **87** (2001) 047003.
- 38) D. L. Feng, D. H. Lu, K. M. Shen, C. Kim, H. Eisaki, A. Damascelli, R. Yoshizaki, J. i. Shimoyama, K. Kishio, G. D. Gu, S. Oh, A. Andrus, J. O'Donnell, J. N. Eckstein, and Z.-X. Shen: *Science* **289** (2000) 277.
- 39) I. M. Vishik, E. A. Nowadnick, W. S. Lee, Z. X. Shen, B. Moritz, T. P. Devereaux, K. Tanaka, T. Sasagawa, and T. Fujii: *Nature Phys.* **5** (2009) 718.
- 40) J. Meng, G. Liu, W. Zhang, L. Zhao, H. Liu, X. Jia, D. Mu, S. Liu, X. Dong, J. Zhang, W. Lu, G. Wang, Y. Zhou, Y. Zhu, X. Wang, Z. Xu, C. Chen, and X. J. Zhou: *Nature* **462** (2009) 335.
- 41) H.-B. Yang, J. D. Rameau, P. D. Johnson, T. Valla, A. Tsvelik, and G. D. Gu: *Nature* **456** (2008) 77.
- 42) A. Kanigel, M. R. Norman, M. Randeria, U. Chatterjee, S. Souma, A. Kaminski, H. M. Fretwell, S. Rosenkranz, M. Shi, T. Sato, T. Takahashi, Z. Z. Li, H. Raffy, K. Kadowaki, D. Hinks, L. Ozyuzer, and J. C. Campuzano: *Nature Physics* **2** (2006) 447.
- 43) S. Ideta, T. Yoshida, A. Fujimori, H. Anzai, T. Fujita, A. Ino, M. Arita, H. Namatame, M. Taniguchi, Z.-X. Shen, K. Takashima, K. M. Kojima, and S. Uchida: arXiv:1104.0313 (unpublished) .
- 44) J. Meng, W. Zhang, G. Liu, L. Zhao, H. Liu, X. Jia, W. Lu, X. Dong, G. Wang, H. Zhang, Y. Zhou, Y. Zhu, X. Wang, Z. Zhao, Z. Xu, C. Chen, and X. J. Zhou: *Phys. Rev. B* **79** (2009) 024514.
- 45) J.-H. Ma, Z.-H. Pan, F. C. Niestemski, M. Neupane, Y.-M. Xu, P. Richard, K. Nakayama, T. Sato, T. Takahashi, H.-Q. Luo, L. Fang, H.-H. Wen, Z. Wang, H. Ding, and V. Madhavan: *Phys. Rev. Lett.* **101** (2008) 207002.
- 46) R.-H. He, M. Hashimoto, H. Karapetyan, J. D. Koralek, J. P. Hinton, J. P. Testaud, V. Nathan,

- Y. Yoshida, H. Yao, K. Tanaka, W. Meevasana, R. G. Moore, D. H. Lu, S.-K. Mo, M. Ishikado, H. Eisaki, Z. Hussain, T. P. Devereaux, S. A. Kivelson, J. Orenstein, A. Kapitulnik, and Z.-X. Shen: *Science* **331** (2011) 1579.
- 47) M. J. Lawler, K. Fujita, J. Lee, A. R. Schmidt, Y. Kohsaka, C. K. Kim, H. Eisaki, S. Uchida, J. C. Davis, J. P. Sethna, and E.-A. Kim: *Nature* **466** (2010) 347.
- 48) Y. J. Uemura, G. M. Luke, B. J. Sternlieb, J. H. Brewer, J. F. Carolan, W. N. Hardy, R. Kadono, J. R. Kempton, R. F. Kiefl, S. R. Kreitzman, P. Mulhern, T. M. Riseman, D. L. Williams, B. X. Yang, S. Uchida, H. Takagi, J. Gopalakrishnan, A. W. Sleight, M. A. Subramanian, C. L. Chien, M. Z. Cieplak, G. Xiao, V. Y. Lee, B. W. Statt, C. E. Stronach, W. J. Kossler, and X. H. Yu: *Phys. Rev. Lett.* **62** (1989) 2317.
- 49) J. L. Tallon, J. W. Loram, J. R. Cooper, C. Panagopoulos, and C. Bernhard: *Phys. Rev. B* **68** (2003) 180501.
- 50) D. B. Tanner, H. L. Liu, M. A. Quijada, A. M. Zibold, H. Berger, R. J. Kelley, M. Onellion, F. C. Chou, D. C. Johnston, J. P. Rice, D. M. Ginsberg, and J. T. Markert: *Physica B* **244** (1998) 1.
- 51) H. Won and K. Maki: *Phys. Rev. B* **49** (1994) 1397.
- 52) H. Ding, J. R. Engelbrecht, Z. Wang, J. C. Campuzano, S.-C. Wang, H.-B. Yang, R. Rogan, T. Takahashi, K. Kadowaki, and D. G. Hinks: *Phys. Rev. Lett.* **87** (2001) 227001.
- 53) D. L. Feng, N. P. Armitage, D. H. Lu, A. Damascelli, J. P. Hu, P. Bogdanov, A. Lanzara, F. Ronning, K. M. Shen, H. Eisaki, C. Kim, J. i. Shimoyama, K. Kishio, and Z.-X. Shen: *Phys. Rev. Lett.* **86** (2001) 5550.
- 54) Z. Konstantinovic, Z. Z. Li, and H. Raffy: *Physica C* **341-348** (2000) 859.